Journal Pre-proofs

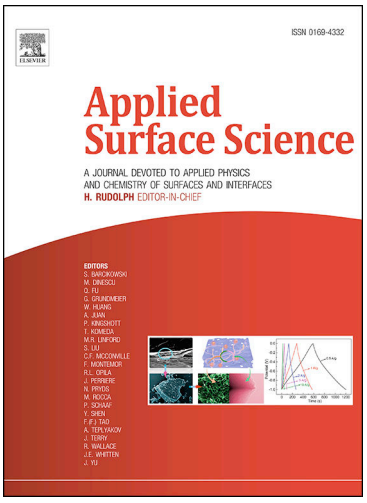

Full Length Article

Polyfluoroalkyl-silica porous coatings with high antireflection properties and low surface free energy for glass in solar energy application

Cecilia Agustín-Sáenz, Maider Machado, Agnieszka Tercjak

PII: S0169-4332(19)33681-5
DOI: https://doi.org/10.1016/j.apsusc.2019.144864
Reference: APSUSC 144864

To appear in: *Applied Surface Science*

Received Date: 22 February 2019
Revised Date: 14 November 2019
Accepted Date: 23 November 2019

Please cite this article as: C. Agustín-Sáenz, M. Machado, A. Tercjak, Polyfluoroalkyl-silica porous coatings with high antireflection properties and low surface free energy for glass in solar energy application, *Applied Surface Science* (2019), doi: https://doi.org/10.1016/j.apsusc.2019.144864

Polyfluoroalkyl-silica porous coatings with high antireflection properties and low surface free energy for glass in solar energy application

Authors:

Cecilia Agustín-Sáenz* (a), Maider Machado (a), Agnieszka Tercjak (b)

Address:

(a) TECNALIA (Energy and Environment Division) - Parque Científico y Tecnológico de Gipuzkoa, Mikeletegi Pasealekua 2, 20009 Donostia - San Sebastián, Spain
(b) Group `Materials + Technologies´ (GMT), Department of Chemical and Environmental Engineering, Faculty of Engineering, Gipuzkoa, University of the Basque Country (UPV/EHU), Plaza Europa 1, 20018 Donostia-San Sebastián, Spain

*Corresponding autor:

Cecilia Agustín-Sáenz
https://orcid.org/0000-0003-1210-9727
Postal address: Mikeletegi Pasealekua 2, 20009 Donostia - San Sebastián, Spain.
Tel.: +34 667 115 865
e-mail address: cecilia.agustin@tecnalia.com

***Keywords**:* antireflective; sol-gel; fluoroalkyl; photovoltaics; soiling; surface energy

Graphical abstract

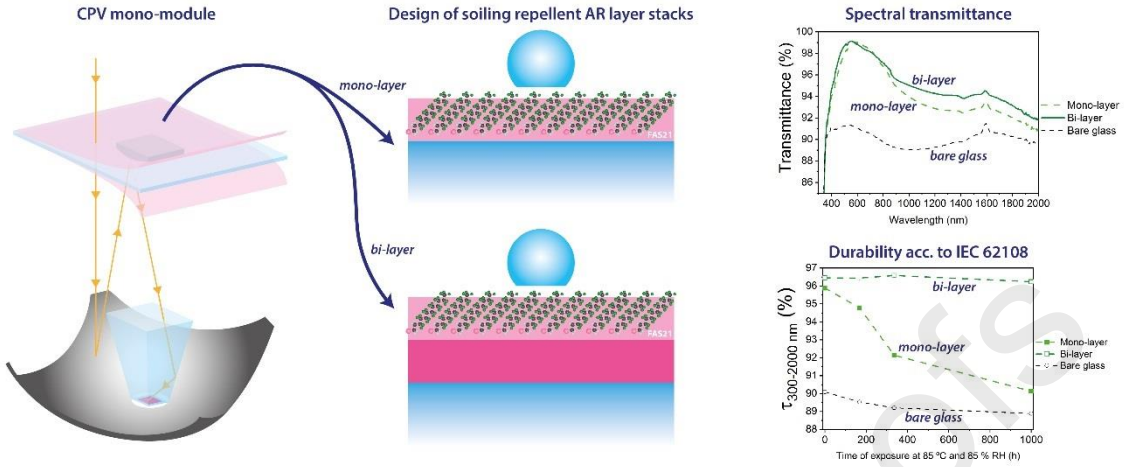

Abstract

Polyfluoroalkyl-silica porous coating stacks with durable antireflection (AR) properties have been obtained for photovoltaic (PV) application. An acid-catalyzed sol-gel process combined with evaporation induced self-assembly and the presence of a non-hydrolyzable polyfluoroalkyl group linked to the central atom of the silicon alkoxide was conducted. The aim was to obtain a low surface energy coating, devised to mitigate soiling adherence, without losing the AR properties of a baseline coating. In particular, the influence of polyfluoroalkyl chain length on the thickness, the water contact angle and optical transmission properties was first analyzed. The optimized polyfluoroalkyl-silica porous coating presented low surface energy < 20 mJ/m^2, even with the desired low roughness values required for obtaining a negligible scattering of the incoming solar radiation. This coating was studied as an AR mono-layer and as an external coating in an AR bi-layer stack, with the presence of an inner dense-structured silica layer, that contributed to both the optical performance and durability, acting as an alkali diffusion preventing layer. The AR bi-layer stack deposited on two sides of glass provided a transmittance gain of 7.1 %. Those optical properties were inalterable after accelerated aging tests, which sustains the reliability of the materials for solar energy applications.

1. INTRODUCTION

Glass is used extensively in solar energy module assemblies due to its optical properties as well as its outstanding mechanical and thermal stability, which provide the necessary protection and insulation required to withstand harsh environmental conditions [1]. However, there are inherent optical losses due to the difference between the refractive indexes of glass and the surrounding medium, typically air. Optical transmission properties of glass can be enhanced by means of antireflective (AR) coating systems that reduce the Fresnel reflection losses [2–4] of the air-glass interface. The tailoring of the refractive index and thickness of an interposed thin coating allows the reflection from the interface to be minimized.

Optical durability is also a key issue to consider when designing AR coating systems for solar applications, since they should be capable of withstanding prolonged exposure in open air climates, including desert and tropical ones [5][6]. Furthermore, they must be able to mitigate the impact of external factors such as dust and dirt adherence that would lead to a reduction of the optical performance of the glass and, therefore, the photovoltaic (PV) system. In particular, concentrated photovoltaic systems (CPV) collect sunlight through optical components (mirrors or lenses) to focus it onto multijunction III-V cells [5][7], and only the direct beam component can be exploited in contrast to flat panels. When the collector surface is soiled, a significant part of the light is scattered and thus, lost. The efficiency of CPV systems is therefore more sensitive to soiling than non-concentrated ones, with more severe associated energy losses [5]. Thus, surface treatments combining antireflective and anti-soiling (AS) properties are interesting to obtain concentrated photovoltaic modules with high, and durable conversion efficiency [8][9].

The surface energy of the coatings is an important property that influences the material's wettability, adhesion and friction properties and therefore it may be modulated to contribute against soiling adherence. In particular, the wetting behavior of a surface by a liquid is

governed by both the surface free energy and its structure [10]. Perfluorinated polymers are known for being materials with extremely low surface free energy, which results in an anti-adhesive behavior for polar and non-polar substances [11]. Shafrin et al. [12] reviewed the critical surface tension exhibited by low energy surfaces. They obtained the following order for those constituted by $-CF_3$ < $-CF_2H$ < $-CF_2-$ < $-CH_2-CF_3$ < $-CF_2-CFH-$ < $-CH_3$ < $-CF_2-CH_2-$ < $-CFH-CH_2-$ < $-CH_2-$. Chlorocarbon or nitrated hydrocarbon surfaces were subsequently ranked after these fluoro and hydrofluoro-carbon based materials. Furthermore, the high strength of the C–F bond grants excellent thermal, chemical, photochemical and hydrolytic stability, which are relevant features for outdoor application and weathering resistance.

In the highly competitive energy market, solar energy emerges as the most promising renewable energy source capable of attaining competitive prices on a large scale due to the drop in total costs and the improvement of the energy yields in recent years. In high direct irradiation conditions, CPV has the potential to provide electricity at competitive costs. To effectively contribute to improving the levelized cost of energy, the efforts focused on the development of highly efficient solar cells must be accompanied by the proper selection of module materials to minimize the optical and electrical losses from cell to module, through cost-competitive solutions. In this scenario, the AR and AS layer system should be deposited by means of a cost-competitive, easy up-scaling, highly efficient as well as environmental-friendly process. The sol-gel method emerges as being among the most attractive processes to meet these targets. This chemical process can be precisely optimized in order to find the synthesis conditions that lead to stable sols with extended pot life that enable mechanically stable coatings with durable AR properties to be deposited, with a high repeatability over time. The synthesis route for the creation of inorganic oxides consists of the admixture of chemical precursors, generally metal alkoxides, that are hydrolyzed with acidic or basic water in alcohol media as a homogenizing agent, obtaining an inorganic network. The presence of amphiphiles

serves to form micelles that act as a template for the inorganic network growth, as first evidenced through the evaporation induced self-assembly (EISA) method by Asefa et al. [13] and Brinker et al. [14]. A mesoporous structure with controlled porosity and refractive index is obtained after calcination of the amphiphiles. Sol-gel processing also offers the ability to synergistically combine inorganic and organic moieties, forming hybrid materials at molecular level when precursors with non-hydrolyzable group linked to the alkoxide central atom are present.

Polyfluoroalkyl alkoxy silanes (FAS) can be used as fluorocarbon moiety carriers in a sol-gel synthetized material. There are several works that have combined FAS in a sol-gel matrix with the aim of obtaining super-liquid-repellent surfaces. Hikita et al. [15] synthetized a coating based on acid catalysis of tetraethyl ortho silicate (TEOS) and triethoxy-1H,1H,2H,2H-perfluorodecylsilane (FAS17), also containing commercial silica nanoparticles in order to control surface roughness. Nakajima et al. [16] prepared a bi-layer formed by an inner acid-catalyzed TEOS combined with acrylic polymer and an external acid-catalyzed FAS17. In a similar way, Bharathibai et al. [17] prepared an inner layer based on TEOS and polydimethylsiloxane resins (PDMS) that was then sprayed with hydrolyzed and unhydrolyzed triethoxy-1H,1H,2H,2H-perfluorooctylsilane (FAS13) sols.

It is well known that the wetting of a surface by a liquid is affected by the roughness of the surface [18–20]. Indeed, an effective way to enhance the hydrophobic properties of a coating is to increase its surface roughness, as corroborated by Miller et al. on polytetrafluroethylene (PTFE) thin films [21]. In this work, the smoother PTFE surface exhibited hydrophobic behavior (90 – 100º) while superhydrophobic properties (150º) were achieved by the roughest surface. However, surface roughness has a remarkable effect on the specular and diffuse components of reflectance. It is known that a smooth surface reflects most of the incident light in the specular direction, whereas a rough surface reflects it in a lobe around the specular

direction [22]. As previously mentioned, CPV technology uses only the direct beam component of the incident light. Thus, diffuse reflection should be avoided.

In previous works [4][23][24], a broadband AR multi-layer was obtained through the combination of silica coatings with controlled thickness and refractive index, by tailoring its dense and porous structures. An acid-catalyzed sol-gel approach combined with a diblock copolymer as a structure directing agent (SDA) resulted in an appropriate method to control the microstructure, pore volume and pore size of the coating while obtaining highly stable sols and materials, thus offering an easy up-scaling technique for AR coating deposition and a highly efficient process.

The main drawback of this method comes from the residual silanol groups (Si-OH) standing on the surface of the external porous silica coating, which are prone to adsorb moisture or contaminants when exposed outdoors. In this work, the combination of AR and soiling repellent properties were intended to be implemented together in a one-step process through the search of low surface energy and a smooth coating in a manner that the outstanding AR properties of the baseline coating are not affected. Modified alkoxy silanes with non-hydrolyzable polyfluoroalkyl groups of several chain lengths have been admixed with TEOS and further hydrolyzed by acid catalysis in the presence of a diblock copolymer as an SDA. To the authors best knowledge, there are very few studies in which the combination of FAS as precursors in sol-gel and EISA synthesis enable the tailoring of a highly antireflective and low surface energy coating for solar energy applications. In this work, the influence of the polyfluoroalkyl chain length and the applied temperature on the water contact angle, thickness and optical properties has been studied to optimize the FAS presence in a porous coating. The effect of the FAS incorporation on the porosity, water adsorption, surface energy and roughness has been assessed and the durability of the best candidates has been validated according to the most relevant tests from photovoltaics standards [25].

2. EXPERIMENTAL PROCEDURE

2.1.Materials

Absolute ethanol (99.9 % purity) and precursor tetraethyl orthosilicate (TEOS, 98 % purity) were purchased from Scharlau and Acros, respectively. Polyfluoroalkylsilanes (3, 3, 3-trifluoropropyl) trimethoxy silane, $CF_3CH_2CH_2Si(OCH_3)_3$ (FAS3, ≥ 97 % purity) and (1H, 1H, 2H, 2H-perfluorooctyl) triethoxy silane, $CF_3(CF_2)_5CH_2CH_2Si(OC_2H_5)_3$ (FAS13, 98 % purity) were purchased from Sigma-Aldrich while (1H,1H,2H,2H-perfluorododec-1-yl) triethoxy silane, $CF_3(CF_2)_9CH_2CH_2Si(OC_2H_5)_3$ (FAS21) was purchased from Apollo Scientific. All of these were used as received. The term polyfluoroalkyl has been used herein according to the terminology recommended by Buck et al. [26]. Polyfluoroalkyl substances are defined as aliphatic substances for which all H atoms attached to at least one (but not all) C atoms have been replaced by F atoms in contrast to perfluoroalkyl moiety in which all the H atoms attached to all C atoms are replaced by F atoms.

Catalyst hydrochloric acid (HCl, 37 % vol) was purchased from Scharlau and was used to prepare a 0.1 M solution in distilled water. The organic structure directing agent (SDA) used was the diblock copolymer polyethylene glycol hexadecyl ether, of an average molecular weight ~ 1124 g/mol. It was purchased from Sigma-Aldrich and used as received.

The low iron float glass used was 4 mm thick Optiwhite® from Pilkington.

2.2.Preparation of sols

Polyfluoroalkyl-silica sols were prepared via acid catalysis following a two-step procedure. During the first step, TEOS, FAS, ethanol, acidified water and SDA were mixed and stirred for 90 min at 80 ºC. Three types of FAS with different chain lengths $-CH_2CH_2–(CF_2)_n-CF_3$ were used to prepare different sols, with n = 0, 5 or 9. Voorhoeve [27] had proved that

organohalosilanes with fluorine in the α- and β-carbon positions to silicon hydrolyzed very easily at the -C-Si≡ bond. For that reason, polyfluoroalkyl with hydrogen in α- and β-carbon and fully fluorinated carbon from the γ-position to the end of the chain were selected since the aim was to synthesize a covalently bonded organic-inorganic hybrid material.

In a second step, a mixture of ethanol and acidified water (0.1 M HCl) was added drop by drop to the solution and was stirred for 60 min at 40 ºC. The resultant sols were aged in sealed glass containers for 2 days. Different equivalent concentrations of SiO_2 were prepared by varying the ethanol/TEOS ratio (R_{Et}). Table 1 summarizes all the formulations used.

Moreover, polyfluoroalkyl-silica sol without SDA content was prepared for growing polyfluoroalkyl-silica dense coating for comparison. Baseline sol with SDA but without FAS content was prepared for growing silica porous coating also for comparison. Silica sol with neither FAS nor SDA content was prepared for growing pure silica dense coating.

Table 1.

Polyfluoroalkyl-silica-porogen sol formulations and temperature applied to derived coatings.

Molar ratio TEOS : FAS : SDA : H_2O : EtOH	**SiO_2 concentration**	**Type of FAS**	**Applied temperature (ºC)**
1 : 0.01 : 0.12 : 8 : 24.4	C1	FAS3	200, 240
1 : 0.01 : 0.12 : 8 : 24.4	C1	FAS13	200, 240
1 : 0.01 : 0.12 : 8 : 24.4	C1	FAS21	200, 240, 350
1 : 0.01 : 0.12 : 8 : 34	C2	FAS21	200, 240

2.3.Preparation of mono- and bi-layers

Polyfluoroalkyl-silica sols were deposited on the 4 mm thick low iron float glass specimens after being cleaned in ethanol under sonication for 15 min and then air dried. Coating deposition was performed on both sides of the low iron float glass by dipping at a controlled withdrawal rate of 5 cm/min under controlled environmental conditions of 22 ºC and 60 % relative humidity (RH). After coating deposition, thermal treatment was performed in a

conventional furnace between 200 – 350 ºC for 1 hour as described in Table 1, followed by ethanol-water cleaning in an ultrasonic bath in order to extract surfactant traces.

AR mono- and bi-layer stacks had been theoretically designed in a previous work [4] through the optimization of the reflectance in a broadband region of the solar spectrum. The thickness, refractive index and porosity of the layers partaking in the optimized AR layer stacks were obtained. The most convenient AR system was a bi-layer stack composed of a dense-structured inner layer with 1.41 refractive index at 700 nm and ~110 nm thick and a porous external layer with a 1.22 refractive index at 700 nm and ~120 nm thick. Furthermore, although covering a narrower spectral bandwidth, the porous external coating was able to provide antireflection properties acting as a single AR mono-layer.

Therefore, optimized polyfluoroalkyl-silica porous coatings were studied as single AR mono-layers and as AR bi-layers stacked on both sides of low iron float glass according to Table 2. To be more precise, the bi-layer stacks were formed by an inner dense coating derived from silica sol dipping at a withdrawal rate of 5 cm/min, sintered at 550 ºC for 1 hour, sequentially followed by an external porous coating derived from FAS21-C2 dipping at a withdrawal rate of 5 cm/min, under controlled environmental conditions of 22 ºC and 60 % relative humidity. After FAS21-C2 deposition, thermal treatment was performed in a conventional furnace between 200 – 240 ºC for 1 hour, also followed by ethanol-water extraction.

Table 2.

Deposition sequence for AR layer stacks preparation.

Reference	Deposition sequence	AR layer stack
F200	FAS21-C2 sol treated at 200 ºC	Mono-layer
F240	FAS21-C2 sol treated at 240 ºC	Mono-layer
D5F200	Silica sol sintered at 550 ºC	Bi-layer

	FAS21-C2 sol treated at 200 ºC	
D5F240	Silica sol sintered at 550 ºC FAS21-C2 sol treated at 240 ºC	Bi-layer

2.4.Characterization

The contact angle was determined by the static drop method, using a Digidrop Contact Angle Meter (GBX Instruments). Ten measurements of the apparent contact angle were taken for water ($\theta_c^{H_2O}$), methanol (θ_c^{MeOH}) and hexadecane ($\theta_c^{C_{16}H_{34}}$). Surface free energy (SFE) was calculated using mean contact angle values by the Owens-Wendt method [28] which has been shown to be highly accurate [29] compared to thermodynamically based empirical equations of state for solid-liquid interfacial tensions.

Coatings thickness was measured using a contact profilometrer Dektak 150. Coatings were scratched with a pin before thermal treatment. After thermal treatment, five scans were taken crossing the scratch along 50 mm. Thickness was determined by calculation of the step height. Total transmittance and reflectance spectra of investigated AR coating stacks were measured with a Jasco V-670 UV-Vis-NIR spectrophotometer equipped with a 150 mm integrating sphere. Reflectance was measured at an incident angle of 8º. Diffuse reflectance spectra were taken by removing the specular component port of the integrating sphere. All spectra were taken in the 300 - 2000 nm wavelength range. Integrated transmittance (τ) was calculated by weighting transmittance values with AM1.5 solar spectral irradiance [30] according to Equation 1.

$$\tau = \frac{\int_{\lambda_1}^{\lambda_2} T_\lambda \cdot S_\lambda d\lambda}{\int_{\lambda_1}^{\lambda_2} S_\lambda d\lambda} \qquad \text{Equation 1}$$

where T_λ is the transmittance spectrum of the coated glass, S_λ is the AM1.5 solar spectrum [30] and λ_1 and λ_2 define the wavelength range where τ is calculated. Integrated reflectance

(ρ) was calculated in a similar way using the measured reflectance spectrum.

The kinematic viscosity of the sols was measured at 22 ºC by means of an Ubbelohde viscometer in which the liquid flows through a capillary tube due to gravity. A type 0B capillary tube was used for sols, since the kinematic viscosity was between 1-5 cSt. Dynamic viscosity (μ) was obtained by multiplying the kinematic viscosity by the density values.

Ellipsometric parameters ψ and Δ, which are functions of the complex refractive index ($\tilde{n} = n + i\kappa$), were recorded by a variable angle spectroscopic ellipsometer (M-2000UTM, J.A. Co., Woollam). Spectra were recorded from 300 to 1000 nm at three incidence angles (50º, 60º, 70º) that were chosen above and below Brewster's angle (angle of vanishing reflection of p-wave, which is ≈ 57º for glass [31]) to ensure a maximum difference in the amplitudes of p- and s-waves. The spectra were fitted using both the dispersion Cauchy model [32] and Bruggeman effective medium approximation (BEMA) model [33]. Thus, the fitting enabled the calculation of parameters such as refractive index (n), extinction coefficient (κ), coating thickness (d) and the porosity. The apparent porosity was calculated with respect to pure dense silica and the void fraction was calculated with respect to the reference dense material. A polarization factor of 0.33 was considered for these calculations. The data analysis was performed with WVase32 software.

Water adsorption-desorption was studied by environmental ellipsometric porosimetry (EEP) [34][35]. Measurements were performed with the equipment described above (M-2000UTM, J.A. Co., Woollam), within a cell with controlled relative humidity. In this case, the spectra were taken at a fixed incident angle of 70 º, at different RH values. Using the Cauchy fitting model, n values were obtained as a function of RH. The absorption-desorption isotherms were calculated by BEMA fitting, using the optical characteristics of the reference dense material.

The surface of investigated coatings was analyzed using atomic force microscopy (AFM). AFM phase and height images were collected by operating in tapping mode with a scanning

probe microscope Multimode 8 from Bruker with Nanoscope V controller. The AFM was equipped with an integrated silicon tip/cantilever with a resonance frequency of ~300 kHz and 42 N m^{-1} spring constant. Scan rates ranged from 0.7 to 1.2 Hz s^{-1}. In order to get repeatable results, different regions of the investigated coatings were scanned to choose representative AFM images. Height and phase AFM images were very similar, thus only AFM phase images are shown here. The roughness of each investigated coating was measured using AFM height images (5 μm x 5μm) and the root mean square value (R_q) is presented.

A damp heat (DH) accelerated aging test was performed following the IEC-62108 CPV standard [25]. The specimens were exposed for 1000 h in a climatic chamber at 85 ºC and 85 % relative humidity conditions. Spectrophotometry, ellipsometry and $\theta_c^{H_2O}$ measurements were carried out at different exposure times to monitor the aging.

A thermal cycling test was performed following the IEC-62108 CPV standard. The specimens were subjected to 400 cycles consisting of 3 h from -40 to 85 °C, and a dwell time of 10 min at the highest and lowest temperatures. Spectrophotometry before and after testing allowed the integrated transmittance loss (τ_{loss}) in the 300 - 2000 nm wavelength range to be calculated.

A humidity freezing test was performed following the IEC-62108 CPV standard. The specimens underwent a warming cycle at a temperature of 85 °C and high RH followed by a fast cooling cycle at very low temperature (-40 °C). Spectrophotometry before and after testing allowed the τ_{loss} in the 300 - 2000 nm wavelength range to be calculated.

For the ultraviolet (UV) aging test the specimens were irradiated by UV light at a constant temperature of 60±5 °C by 7.5 kWh/m^2 in the range 280-320 nm and by 15 kWh/m^2 in the range 320-400 nm. The total test duration was 96 h. Spectrophotometry before and after testing allowed the τ_{loss} in the 300 - 2000 nm wavelength range to be calculated.

3. RESULTS AND DISCUSSION

3.1.Effect of polyfluoroalkyl chain length on wettability, thickness and optical properties.

First, the effect of adding three FAS during sol preparation with the aim to introduce polyfluoroalkyl chains with different length in a previously known AR coating material [24] was studied. The coatings grown with this baseline silica formulation (acid-hydrolyzed TEOS in excess water in the presence of diblock copolymer and R_{Et} equal to C1) were 125-130 nm thick with a refractive index equal to 1.22 at 700 nm. With these features, the baseline coating deposited on both sides of low iron float glass revealed $\tau_{300\text{-}2000nm}$ up to 96.3 % and $\theta_c^{H_2O} < 20^o$. In order to preserve the outstanding transmittance values provided by the baseline coating, FAS was introduced in the sol in a FAS/TEOS ratio as low as 0.01 to attain repellent coatings. As explained before, the three types of polyfluoroalkyl silicon alkoxides were introduced in the same molar ratio (1 TEOS : 0.01 FAS) during the baseline sol preparation, with the same R_{Et} (C1). This, therefore, permitted the incorporation of the following polyfluoroalkyl chains covalently bonded to a porous silica backbone: $–(CH_2)_2–CF_3$; $–(CH_2)_2–(CF_2)_5–CF_3$ and $–(CH_2)_2–(CF_2)_9–CF_3$ with the presence of similar concentrations of terminal $–CF_3$ groups in all the prepared coating materials. As explained before, Shafrin et al. [12][36] postulated that the non-wettable surface with the lowest surface energy is ideally comprised of closely packed $–CF_3$ groups. Therefore, wettability appears to be less related to the polyfluoroalkyl chain length itself and more to its proper orientation to yield total exposure of $–CF_3$ moieties. The effect of the addition of these moieties in the $\theta_c^{H_2O}$ of the coatings treated at several temperatures is displayed in Figure 1a. One can easily observe that the polyfluoroalkyl chain length plays a role in the configuration of the investigated coatings, since a higher $\theta_c^{H_2O}$ was exhibited as the chain length increased. In the case of organic surfaces, the wettability is generally given by the nature and packing of the exposed atoms or groups and tends to be independent of the arrangements of the underlying molecules. In the proposed approach, in which FAS compounds were added in low TEOS : FAS molar rate, the longer the fluoroalkyl

chain was embedded in the coating, the more possibilities the $–CF_3$ moieties had to emerge from the surface. Therefore, in this case, the fluoroalkyl chain length was crucial for obtaining non-wettable surfaces with such a low TEOS : FAS molar rate contained in the material. It is well known that fluoropolymers composed of perfluoroalkyl chain $–(CF_2)_n–$ show the best resistance to high temperatures, up to 260 ºC, thanks to the strength of the C-F bond. In any case, the rate of decomposition depends on the particular matrix, as well as the temperature and the exposure time. As observed in Figure 1a, $\theta_c^{H_2O}$ of the coatings treated at 200 and 240 ºC were of the same order for the same coating material. The water contact angle values were ~108º and ~105º for $–(CH_2)_2–(CF_2)_9–CF_3$ (FAS21), treated at 200 and 240 ºC, respectively, while they dropped to ~70º for the coating treated at 350ºC.

As long as the polyfluoroalkyl length chain increased, the thickness of the derived coating also did so. Figure 1b shows the thickness measured by profilometry on coatings treated at 240ºC. The thickness of coating containing $–(CH_2)_2–CF_3$ was close to the baseline thickness, while the coating with $–(CH_2)_2–(CF_2)_9–CF_3$ reached 260 nm. This modification of coating thickness significantly affected the optical properties. The increase of the polyfluoroalkyl length chain acted detrimentally on transmittance as observed in Figure 1c, where its integrated value, $\tau_{300\text{-}2000nm}$ is graphed for coatings sintered at 200, 240 and 350 ºC, before and after ethanol-water extraction. On this occasion, the presence of the same molar ratio of TEOS : FAS led to an increase of the weight ratio (FAS3 < FAS13 < FAS21) and the higher quantity of fluorinated moieties in the baseline coating provoked a reduction of the antireflection properties. Indeed, perfluorinated polymers are known to have high reflectance properties, mostly in the diffuse component [37] and therefore, the FAS addition must be rationally designed.

The difference in transmittance between the same coating material when treated at 200 or 240 ºC was notable for measurements before ethanol-water extraction (solid dots), being higher

for coatings treated at 240 ºC. This fact was attributed to the higher presence of SDA traces on the coating pores treated at 200 ºC. After SDA extraction, coatings treated at 200 and 240 ºC and prepared with the same sol exhibited similar values (hollow dots), being ~96.3 % for FAS3, ~95.0 % for FAS13 and ~94.0 % for FAS21-coatings. At these temperatures, the fluorinated moiety did not suffer degradation, and the effect of its presence was perceived on the low wettability values detected. However, the transmittance of FAS21-coating treated at 350 ºC stood out from those treated at 200 or 240 ºC, reaching 95.2 % against 94.0 %, which may be also related with the gradual decomposition of the fluorinated moiety. This effect was also consistent with the low $\theta_c^{H_2O}$ obtained on this surface. In Figure 2, the transmittance spectra between 300-2000 nm of the fluorinated coatings studied in this Section together with the baseline coating are displayed. Therein, the similarity between baseline and FAS3-coating spectra evinces that the incorporation of a short polyfluoroalkyl chain does not interfere in the thickness nor in the optical properties. However, FAS13- and FAS21-coatings spectra evinced that long polyfluoroalkyl chains had an impact on the thickness and the intrinsic material properties of the baseline coating, thus altering the optimized constructive and destructive interferences of its spectrum. The transmittance of a perfectly smooth coating stacked on glass is described by Fresnel equations, and depends only on its complex refractive index ($\tilde{n} = n + i\kappa$) and thickness. Therefore, the conditions for achieving an optimal tandem must be found. Although only very small amounts of a non-hydrolyzable polyfluoroalkyl chain alkoxy silane were needed to produce hydrophobic porous silica coatings, the coating that displayed the highest $\theta_c^{H_2O}$ value, with the longest fluoroalkyl chain embedded, -CH_2CH_2–$(CF_2)_9$-CF_3, did not show the required antireflective performance. Fluoroalkyl moiety quantity should henceforth be optimized in order to balance low interfacial energy and high antireflection properties in a one-step coating.

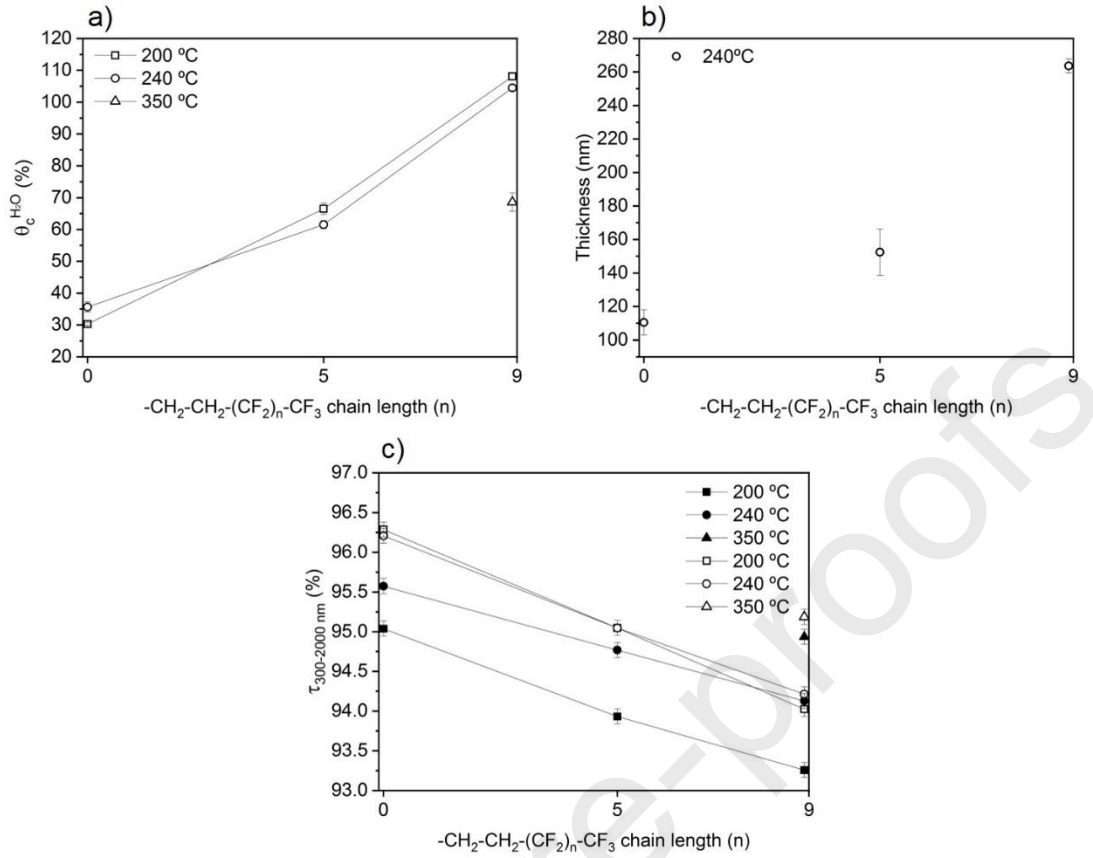

Figure 1. Water contact angle ($\boldsymbol{\theta_c^{H_2O}}$) (a), thickness (b) and integrated transmittance (300-2000 nm) (c), of polyfluoroalkyl-silica porous coatings with different chain length before (solid dots) and after (hollow dots) ethanol-water extraction.

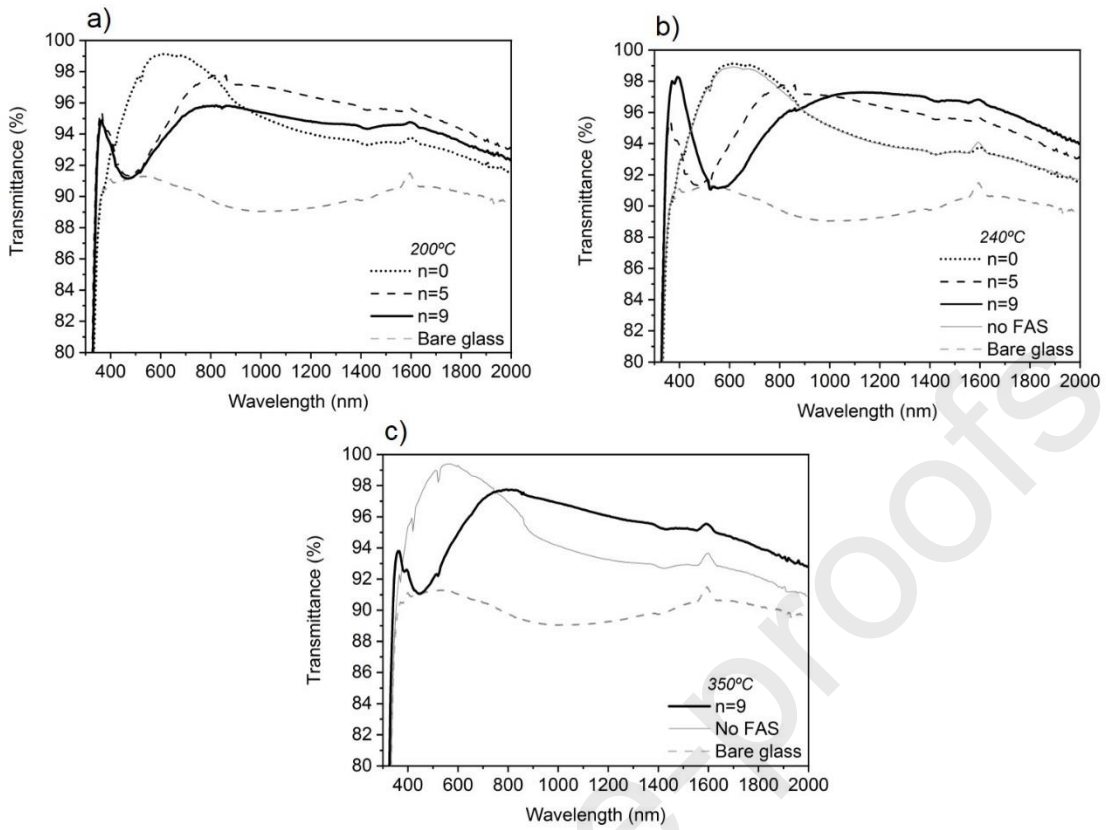

Figure 2. Total transmittance spectra of polyfluoroalkyl-silica porous coatings with different chain length, deposited on both sides of low iron float glass treated at 200 ºC (a), 240 ºC (b) and 350 ºC (c).

3.2.Structural and textural properties of optimized coating with the longest polyfluoroalkyl chain.

Motivated by the promising values of water contact angle obtained with coatings containing a low quantity of the longest polyfluoroalkyl chain-modified alkoxy silane, the FAS21-C1 formulation was adjusted to obtain a thinner coating with outstanding antireflective properties. The optimization of the formulation was accomplished by R_{Et} adjustment with the purpose of interfering in the sol viscosity. The previous addition of FAS21 to baseline formulation implied a viscosity increase from 2.52 ± 0.05 cP to 2.81 ± 0.01 cP. This parameter was then fitted to 2.30 ± 0.04 cP after ethanol addition to obtain FAS21-C2 sol. The stability of the latter sol was excellent since the viscosity remained unchanged after at least one year of aging.

This fact is very encouraging for the implementation and scaling up of the one-step process. Based on the outcome of the optical optimization performed in a previous work [4] which allowed the calculation of the optimal thickness, refractive index and porosity of the coatings composing AR layer stacks (from 1 to 4 layers), FAS21-C2 sol served to grow AR mono- and bi-layer architectures.

On one side, FAS21-C2 sol and a similar sol without SDA were used to grow polyfluoroalkyl-silica porous and dense coatings, respectively, on low iron float glass. The coatings were characterized by spectral ellipsometry before and after thermal treatment (Table 3).

The purpose of the thermal treatment was the elimination of the SDA and the densification of the network by means of the reduction of the skeletal density of the gel to higher crosslinked chains and clusters, with the aim of achieving a stable structure. The presence of SDA in the formulation led to an expansion of the coating thickness before thermal treatment from 90 nm to 500 nm, as presented in Table 3. According to TGA measurements performed in a previous work [24] the temperature at which SDA starts to decompose is 180 ºC and would be expected to be totally decomposed at 350 ºC. However, the coatings treated at this temperature showed a significant decrease of $\theta_c^{H_2O}$, as explained in the previous Section. On the other hand, cover glasses used for solar modules usually need to be tempered in order to achieve higher mechanical strength. This process consists of heating the glass to temperatures around 700 ºC followed by a forced cooling that creates surface and edge compression by air-quenching. The resulting mechanical properties can be undesirably modified if the glass is treated again at high temperatures. In order to avoid this effect, the selected temperature to build the final AR mono- and bi-layer stacks was lower than 240 ºC. Therefore, the ethanol-water extraction step was required to totally remove the SDA from the coating pores. The resultant thickness of the FAS21-silica porous coating treated at 240 ºC was ~ 130 nm as presented in Table 3. During the thermal treatment, the organic phase keeps a fixed coating volume up to 180 ºC when its

decomposition starts. Below that temperature the coating contraction is only due to volumetric contraction of the polyfluoroalkyl-silica material. Above that temperature the thickness shrinkage is due to the sum of the contraction of polyfluoroalkyl-silica walls and the thermal decomposition of the organic phase. It has been postulated [38] that thickness reduction is accompanied by a unidirectional contraction of the domain normal to the surface plane. The thickness of the coating grown with sol without SDA content shrank from ~ 90 nm to ~ 60 nm. This 33 % contraction, that can be mostly attributed to the polyfluoroalkyl-silica phase densification, was useful to identify which part of the 74 % thickness reduction for the coating with SDA came from the material itself. During the thermal treatment, the removal of solvent and water permits crosslinking to continue as unreacted hydroxyl and alkoxy groups come in contact. However, the temperature applied on this occasion was not high enough to allow either the pyrolysis of unhydrolyzed alkoxy groups or the removal of physically absorbed water. The required temperature for achieving the most thermodynamically stable structure is not compatible with the maintenance of fluoroalkyl chains in the final network. Thus, the performance of the material treated at relatively low temperature should be validated under reliability tests in order to verify if the obtained structure is stable enough to endure real operation conditions.

The refractive index after the thermal treatment and water-ethanol extraction of SDA from pores, coincided with the target value, 1.22 (at 700 nm), thereby permitting the optimized transmittance spectrum to be achieved [4]. The porosity, which was calculated by BEMA fitting with the assumption that the network was formed by pure dense silica and voids, was close to 50 %.

On the other hand, after demonstrating its suitability for the AR mono-layer, the FAS21-C2 sol was also used to compose the AR bi-layer stack. A dense silica coating was deposited as inner coating (sintered at 550 ºC) followed by FAS21-C2 deposition to form the external

porous coating. The ellipsometric parameters were also measured and the values obtained from Cauchy and BEMA fitting are summarized in Table 4. The thickness and refractive index obtained for polyfluoroalkyl-silica porous coating were similar to those obtained for the coating directly grown on glass. The morphology of these coatings is presented in Figure 3, where Figure 3a shows the surface of the FAS21 coating deposited directly on glass and Figure 3b corresponds to FAS21 deposited on dense silica coating. Both structures were quite similar and homogeneous, being formed by little grains which differed in size. The coating deposited on glass was formed by grains of 4 ± 2 nm size and the coating deposited on the dense silica coating presented 12 ± 3 nm sized grains. The roughness, R_q, was as low as 0.6 nm in both cases. The surface of FAS21-silica dense coating grown from the sol without SDA showed a different structure (Figure 3c). The morphology of the surface was compact, without grains, holes or pores. However, some white zones throughout the surface which corresponded to differences in height could come from agglomeration or differences in solvent evaporation. The roughness R_q of this sample was 4.5 nm, relatively higher than the values obtained for the porous coatings. Therefore, the presence of SDA, apart from being porogen, also participated in the achievement of homogeneous and smooth surfaces.

The polyfluoroalkyl-silica porous and dense coatings grown on glass were further analyzed by environmental ellipsometric porosimetry (EEP). Refractive index (at 700 nm) was obtained from ellipsometric data fitting recorded at different relative humidity values during the adsorption and desorption steps and depicted in Figure 4a. This enabled the detection of the amount of adsorptive (water vapor) inside pores from the change of optical characteristics of the coatings at several water partial pressures. Adsorption-desorption curves of FAS21-silica porous and dense coatings treated at 240 ºC are shown in Figure 4b. As expected, differences in water absorption between dense and porous coatings were detected due to their different structures. Optical properties of FAS21 dense coating displayed a slight initial increase in the

refractive index that was maintained constant from 10 % RH up to the highest RH conditions. This slight increase at lower RH conditions may be associated with the formation of a water mono-layer on the top of the surface whereas no water adsorption was observed. On the other hand, the porous coatings displayed the typical behavior of mesoporous materials associated with type IV - V isotherms according to IUPAC classification of porous materials. Therefore, according to these measurements, water vapor enters inside the pores of FAS21-silica coating. The real volume of pores, calculated for the FAS21-silica porous coating by taking FAS21-silica dense coating as the reference material, came to 47.5 % and was filled with water vapor at partial pressure > 0.8 as observed in the adsorption-desorption isotherm. Little adsorption was observed at the lower RH conditions, up to capillary adsorption zone, which is characterized by a steep increase of adsorbed volume, detected herein at 60 % RH. During capillary desorption, the decrease of the adsorbed water took place at RH values around 55 %. The differences between adsorption-desorption branches are associated to the difference in the radius of the curvature of the condensed liquid meniscus during the adsorption and desorption processes in the mesopores [35]. The shape of these hysteresis loops may usually be correlated according to an empirical classification in four types of curves (H1 - H4) given by IUPAC. The studied coating was identified as H1, shaped by parallel branches, which are associated to well-defined cylindrical-like pore channels or agglomerates of approximately uniform spheres as displayed by the AFM images of Figure 3.

Table 3.

Refractive index at 700 nm (n), thickness before (d_{raw}) and after thermal treatment (d) and apparent porosity of porous and dense FAS21-silica coating treated at 240 ºC.

Coating	n (700 nm)	d (nm)	d_{raw} (nm)	Apparent porosity (%)

F240	1.22	128.2	500.5	51.3
F240-no SDA	1.42	60.8	89.4	-

Table 4.

Refractive index at 700 nm (n) and thickness (d) of inner and external coatings of the AR bi-layer stack and apparent porosity of the external FAS21-silica coating treated at 240 ºC.

Coating	n_{inner} (700 nm)	d_{inner} (nm)	$n_{external}$ (700 nm)	$d_{external}$ (nm)	Apparent porosity (%)
D5F240	1.46	107.6	1.22	131.1	50.0

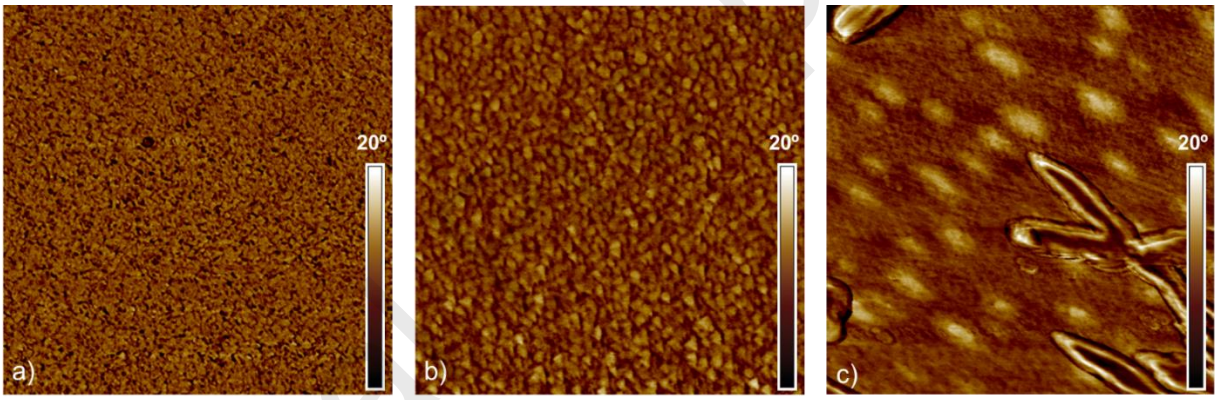

Figure 3. AFM phase images (1 µm x 1 µm) of the FAS21-silica porous mono-layer (a), bi-layer (b) and FAS21-silica dense coating (c) all treated at 240 ºC.

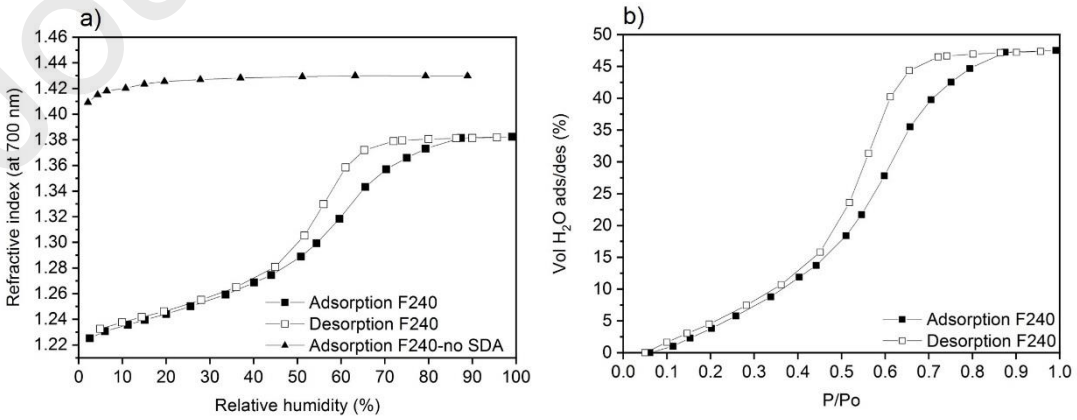

Figure 4. Refractive index (at 700 nm) as a function of relative humidity of FAS21-silica porous and dense coatings (a) and adsorption-desorption isotherm (b) of FAS21-silica porous coating treated at 240 ºC.

3.3.Surface free energy of optimized coating stacks with the longest polyfluoroalkyl chain.

The free energy of a flat and chemically homogeneous surface is given by Young's equation (Equation 2).

$$\gamma_{sl} = \gamma_{sv} - \gamma_{lv}\cos\theta_c \qquad \text{Equation 2}$$

where γ is the SFE, and subscripts sl, sv, and lv refer to the solid–liquid, solid– air, and liquid–air interfaces.

The contact angle value, which is still commonly used as the basis for calculating the SFE [39], can be affected by further phenomena that may occur in the solid-liquid interface such as adsorption, catalysis or wetting. Because of this, some assumptions concerning the relation between γ_{sl}, γ_{sv} and γ_{lv} have been theoretical and empirically developed. In any case, due to the ease of carrying out measurements and the high accuracy of the results, those based on contact angle measurements remain the most widely used.

Several authors following in the steps of Fowkes [40] developed the idea of the partition of the SFE into individual components. The main assumption is that the surface free energy is the sum of independent components, associated with specific interactions such as dispersion, polar, hydrogen bonds, induction or acid-base. Owens and Wendt [28] considered only two phenomena by making a distinction between the weak, dispersive van der Waals forces, called the dispersion component and the stronger hydrogen-bonding forces, associated with the polar interaction, which derived from the relationship presented in Equation 3. In order to solve this equation, the contact angle must be measured using at least two liquids, at least one of which must have a polar part > 0.

The SFE of optimized AR coating stacks was determined by measuring the contact angle of the surface with water (γ_{lv}^{p}=51 mN/m; γ_{lv}^{d}=21.8 mN/m), methanol (γ_{lv}^{p}=4.3 mN/m; γ_{lv}^{d}=18.2 mN/m), and n-hexadecane (γ_{lv}^{p}=0 mN/m; γ_{lv}^{d}=27.5 mN/m). The corresponding contact angle and the surface free energy calculated by Owens-Wendt method are shown in Figure 5. The behavior of porous coatings grown from FAS21-C2 sol treated at 200 and 240 ºC and deposited either directly on low iron float glass (AR mono-layer) or on dense silica inner coating (AR bi-layer) was characterized. Polyfluoroalkyl-silica dense coating treated at 240 ºC was also studied for comparison.

All layer stacks exhibited $\theta_c^{H_2O}$ around 100º. Among the AR layer stacks, the main differences were found between the coatings treated at 200 or 240 ºC. $\theta_c^{H_2O}$ of the mono-layer treated at 200 ºC was ~105º while the one treated at 240 ºC showed ~99º. The bi-layers exhibited a few grades below the values of their mono-layer counterparts.

Polyfluoroalkyl-silica porous coating stacks showed a very low SFE between 17–20 mJ/m^2, depending on thermal treatment. Indeed, stacks treated at 200 ºC exhibited lower SFE values than those treated at 240 ºC. However, the polyfluoroalkyl-silica dense coating presented the lowest surface free energy, 15 mJ/m^2. The surface polarity was in all cases lower than 14 % of the total surface free energy, which meant that the wetting was driven by the weak dispersive molecular interactions [29]. The slight change in the FAS21-silica porous coating structure led by the presence of the inner dense coating, provoked a slight increase on the surface polarity. The polar part of F200 increased from 7.5 to 11 % when the coating was deposited as mono-layer or as external layer in the bi-layer, while F240 experimented an increase from 11.8 to 14 % for similar stackings. Surface energy properties of pure PFTE, highly inert and non-polar, obtained by Wood III et al. [29] applying Owens-Wendt method on a variety of commercial PFTE, were 18.0 mJ/m^2 (total SFE) and 0 mJ/m^2 for the polar component.

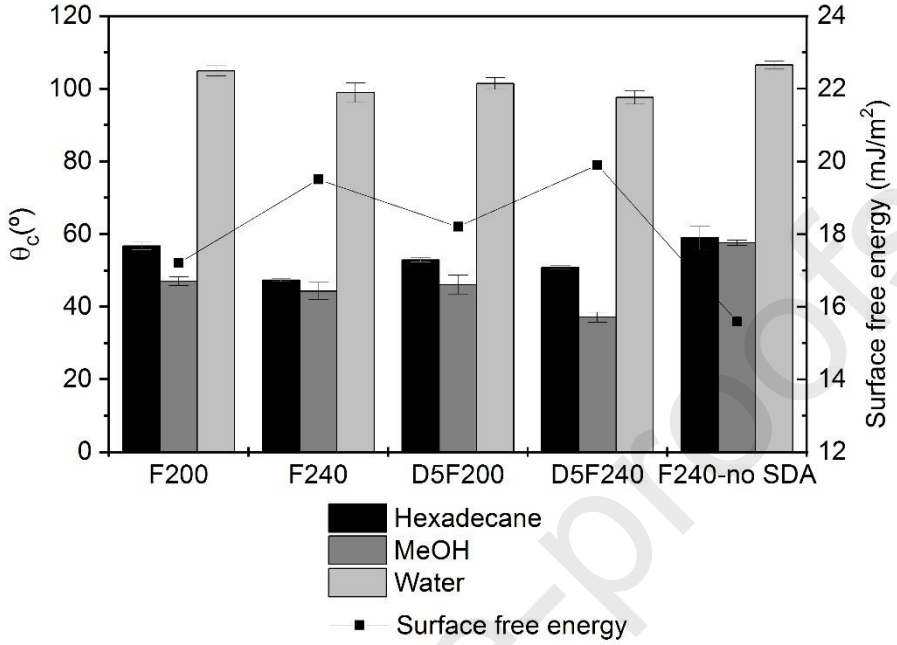

Figure 5. Contact angle ($\boldsymbol{\theta_c}$) of AR layer stacks prepared with FAS21-C2 sol treated at 200 and 240 ºC, with three test liquids and surface free energy.

The SFE values achieved for the optimized AR coating stacks were considered outstanding, taking into account both the low molar quantity of the non-hydrolyzable polyfluoroalkyl silicon alkoxide required and the smoothness exhibited by the coatings, whose roughness is compiled in Table 5.

It is well known that the wetting of a surface by a liquid is strongly affected by its topography [18–20] since surface roughness decreases the spreading of the wetting liquid. Miller et al. [21] prepared PTFE thin films and controlled the roughness R_q at 8 nm and 80 nm (measured by AFM). They observed that roughness strongly influenced the wetting behavior of water at the surface of PTFE thin films. The smother surface permitted hydrophobic behavior to be obtained (90 – 100º) while the roughest surface presented superhydrophobic properties (150º). Considering the $\theta_c^{H_2O}$ achieved for the films with the lowest roughness, formed by such a highly inert and low wettable material, the results obtained herein with such a low

polyfluoralkyl content could not have been better with these low roughness values (R_q < 3.5 nm).

However, as outlined above and discussed in more depth in Section 3.4, roughness is a parameter that also affects optical properties, particularly, light diffusion and scattering [22].

Table 5.

Water contact angle ($\theta_c^{H_2O}$), surface free energy (SFE), their polar and dispersive components and roughness R_q of AR layer stacks.

	$\theta_c^{H_2O}$ (º)	SFE (mJ/m^2)	Polar component (mJ/m^2)	Dispersive component (mJ/m^2)	R_q* (nm)
F200	104.9 ± 1.4	17.2	1.3	15.9	3.5
F240	98.9 ± 2.7	19.5	2.3	17.2	0.6
D5F200	101.4 ± 1.6	18.2	2	16.2	1.4
D5F240	97.6 ± 1.9	19.9	2.8	17.1	0.6
F240-no SDA	106.5 ± 1.0	15.6	1.2	14.4	4.5

*determined by AFM

3.4.Transmittance and reflectance of optimized coating stacks with the longest polyfluoroalkyl chain.

The total transmittance and reflectance spectra as well as the diffuse reflectance are represented in Figure 6 and Figure 7. Figure 6 shows the total transmittance and reflectance of AR mono- and bi-layer stacked on both sides of low iron float glass treated at 200 and 240 ºC, before and after ethanol-water extraction. Figure 7 shows the diffuse reflectance of AR mono- and bi-layer stacked on two sides of low iron float glass. The integrated values in the 300-2000 nm spectral range are compiled in Table 6.

The spectra collected in Figure 6 show how the effect of SDA removal from pores on coatings treated at both temperatures affects mainly the visible bandwidth. This effect is consistently stronger for the stacks treated at 200 ºC.

Mono- and bi-layers treated at 240 ºC provided outstanding transmittance properties in the whole spectral range compared to those treated at 200 ºC, achieving an integral transmittance gain of 6.4 % for the mono-layer and 7.1 % for the bi-layer treated at 240 ºC versus 4.9 % and 5.1 % for mono- and bi-layer stacks treated at 200 ºC. Maximum values were obtained at 575 nm for the AR mono-layers and between 530–555 nm for the case of AR bi-layer stacks. The antireflective behavior obtained by the polyfluoroalkyl-silica AR layer stacks treated at 240 ºC were as outstanding as those obtained by the baseline silica mono- and bi-layer stacks [24]. As proven therein, the presence of the inner dense coating in the bi-layer allows higher values in the NIR bandwidth to be achieved in comparison to the AR mono-layer.

The reflectance of an ideal smooth surface is described by Fresnel equations, and depends only on the complex refractive index ($\tilde{n} = n + i\kappa$) of the incident and exit media as well as the incidence angle. Ginneken et al. [22] developed a reflection model for isotropic rough surfaces based on the local reflection properties of the material and the topography of the material, i.e., the complex refractive index and the roughness, determining the amount of radiation that is reflected in the specular direction or that is diffusely scattered. Surface roughness increases diffuse reflectance, generating a lobe around the specular direction. Additionally, the light transmitted to the bulk of the material and to the external medium after multiple internal reflections produces a diffuse transmittance pattern, which reduces the direct transmittance. Given that concentrated solar systems, in contrast to flat panels [41], only make use of direct solar radiation, the scattering of the incoming solar radiation must be minimized in order to avoid related electrical losses. Consequently, the AR coatings developed herein have been designed to exhibit low roughness, with $\theta_c^{H_2O}$ limited to 100º.

In this case, in which the material is a dielectric composite containing silica, fluorocarbon moiety and voids, diffuse reflectance has been analyzed to discard light scattering coming from differences in phase, especially in view of the high reflectance of pure PFTE [37].

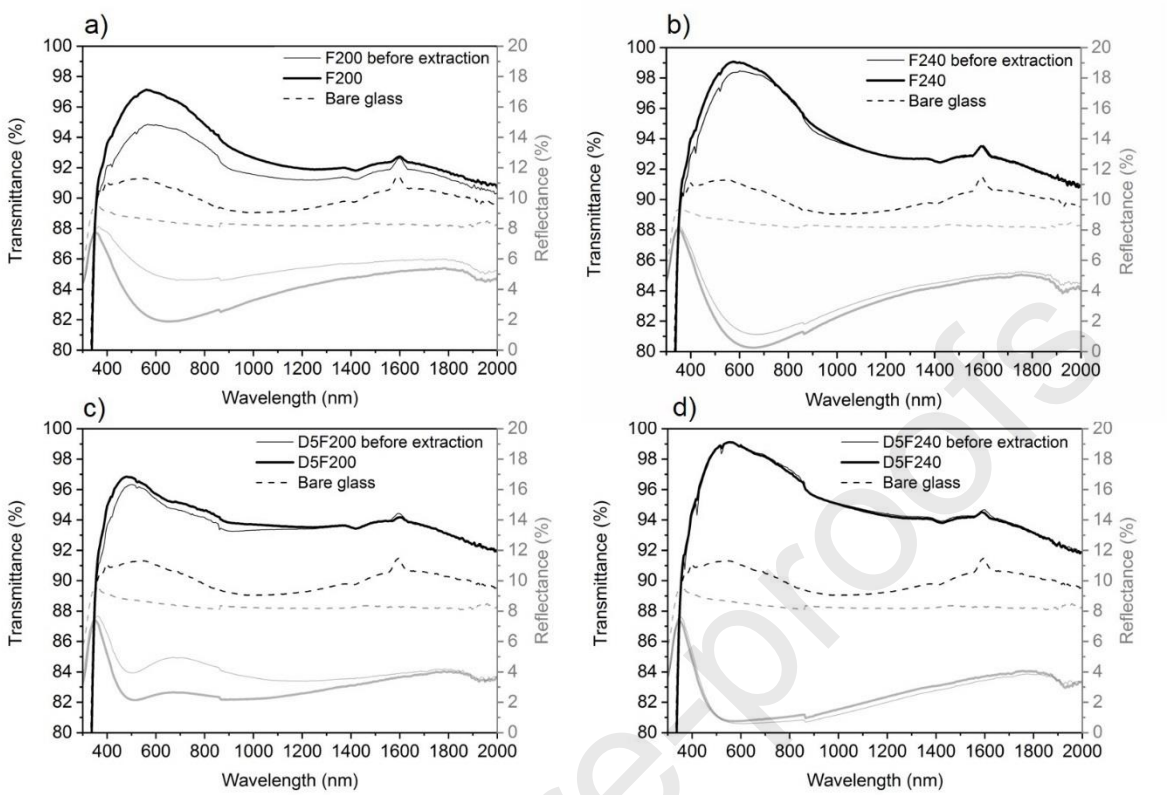

Figure 6. Transmittance and reflectance spectra of AR mono-layer (a, b) and bi-layer (c, d) stacks prepared with FAS21-C2 sol treated at 200 and 240 ºC.

The diffuse reflectance spectra of AR mono- and bi-layers stacked on both sides of glass in Figure 7 show that most part of the diffuse reflectance was produced in the visible range. Furthermore, stacks treated at 200 ºC exhibited higher values over those treated at 240 ºC. Diffuse reflectance values in the 380-780 nm range were around 0.5 % for stacks treated at 200 ºC versus 0.3 % for stacks treated at 240 ºC. As explained before, a higher temperature of the thermal treatment, enables the desirable final material to be obtained, given that removal of solvent and water allows unreacted hydroxyl and alkoxy groups to come into contact.

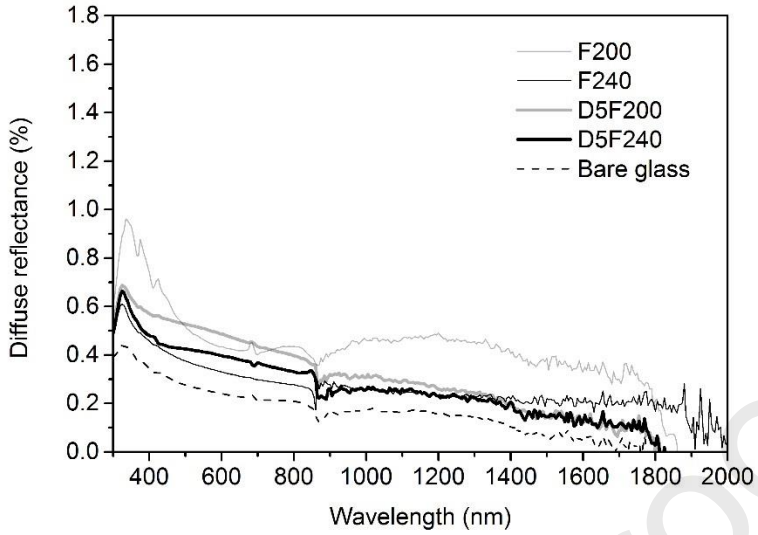

Figure 7. Diffuse reflectance spectra of AR mono-layer and bi-layer stacks prepared with FAS21-C2 sol treated at 200 and 240 ºC.

Table 6.

Total transmittance (τ), total reflectance (ρ) and diffuse reflectance (ρ_{dif}) integrated values in the wavelength range 300-2000 nm of the FAS21-silica AR layers stacked on both sides of low iron float glass.

	τ (%)	**ρ (%)**	**ρ_{dif} (%)**
F200	94.5	3.3	0.5
F240	95.9	2.2	0.3
D5F200	94.7	2.8	0.4
D5F240	96.5	1.8	0.3
Bare glass	90.1	8.5	0.2

3.5.Durability testing

Polyfluoroalkyl-silica AR layer stacks with the most balanced and successful features were tested under accelerated aging conditions designed according to the IEC-62108 standard [25]. This standard is commonly regarded by the CPV industry as a validation of the reliability of materials used for solar system components that have to withstand exposure to harsh climates during their life cycle. Having proven that antireflection properties of FAS21-silica porous coatings treated at 240 ºC were as suitable as the ones displayed by the baseline coating, the next step in this work was aimed to ensure the required long-term durability under the most demanding test of those included in the IEC standard, damp heat exposure [42]. Acknowledging the importance of the sintering temperature in the final properties of the coatings, the design of the thermal treatment for these coatings was based on the contact angle and low surface energy properties. The main objective was to assess the durability of the optical properties of the polyfluoroalkyl-silica coating treated at such a low temperature as part of the AR layer stacks. The bi-layer stack, whose configuration contributes to implementing the broadband antireflection properties, was then considered due to the role of the inner dense coating as an alkali-diffusion barrier, as confirmed in a previous work [43].

The evolution of integrated transmittance values in the 300 – 2000 nm range recorded on mono- and bi-layer stacks with F240 as external coating deposited on both sides of low iron float glass during their exposure in the chamber at 85 ºC/85 % RH is presented in Figure 8. It is observed therein that the mono-layers displayed a constant deterioration of their optical properties throughout the exposure time within the chamber. The behavior of the bi-layer stacks, on the other hand, was outstanding, since the transmittance remained constant throughout exposure, showing no degradation of the optical properties at the end of the test. Indeed, the mono-layers lost 6 % of their initial transmittance while the bi-layers lost a negligible 0.2 % which corresponded to an 8.3 % gain over aged bare glass as reported in Table 7.

The microscope images collected in Figure 10 show the appearance of surfaces before and after exposure of AR mono- and bi-layer to damp heat aging. Fresh coatings presented a smooth and homogenous surface that was altered after ageing. The F240 coating performed in a different way to the stress produced during testing depending on where it was deposited, directly on glass or on the inner dense silica coating. The mono-layer at the end of the test presented circular cracks of 40-100 µm in diameter, showing that forces acting in the coating found the minimization of tension by cracking in a circle shape. However, F240 deposited as external coating on the AR bi-layer stack showed minimum damage after test, which revealed that the cohesion and adhesion forces of polyfluoroalkyl-silica deposited on dense-structured silica were higher and robust enough to withstand the aggressive test conditions.

Coating thickness and refractive index from Cauchy fitting of ellipsometric data as well as $\theta_c^{H_2O}$ after aging are also presented in Table 7. These results were perfectly consistent with the antireflection properties obtained and served to explain the behavior of each layer stack. The F240 mono-layer also suffered a thickness reduction and an increase of its refractive index, probably due to the collapse of the mesostructure, since it would not have achieved the most thermodynamically stable structure at this temperature. However, the external F240 in the bi-layer stack maintained indeed their ellipsometric properties, and thus the optical thickness, refractive index and the porosity of the coating. Therefore, the presence of an inner dense-structured coating sintered at a high temperature had a crucial effect on the durability properties of the polyfluoroalkyl-silica porous coating deposited on it. Apart from the broadband antireflection properties displayed by this stack, the incorporation of the inner layer plays an important role on durability which may be caused by the prevention of alkali diffusion from glass to the porous coating and by the positive effect on the adherence of the external polyfluoroalkyl-silica porous coating. After the damp heat exposure, both mono- and bi-layer stacks displayed $\theta_c^{H_2O}$ values of ~ 113º, slightly higher than initial values.

Total transmittance and reflectance as well as diffuse reflectance of polyfluoroalkyl-silica AR layer stacks after damp heat aging are depicted in Figure 9. Figure 9a shows transmittance and reflectance spectra, respectively, recorded between 300 – 2000 nm for mono- (F240) and bi-layer (D5F240) stacks treated at 240 ºC, while Figure 9c shows the diffuse reflectance spectra for the same AR layer stacks. As expected, transmittance and reflectance spectra of the bi-layer maintained its broadband AR behavior, while mono-layer spectra revealed a loss of optical performance. Diffuse reflectance spectrum of the bi-layer stack showed no changes from the initial one. However, the damage produced in the mono-layer material after aging increased the diffuse reflectance, which reached 0.6 % in the visible wavelength range.

In light of the findings, only the D5F240 bi-layer was subjected to additional aging tests. The transmittance loss induced by ultraviolet, thermal cycling and humidity-freezing tests was below 1 %, which confirmed the outstanding durability and versatility of the polyfluoroalkyl-silica AR bi-layer stack, in relation to its mechanical stability, hydrophobicity and finally its anti-soiling potential.

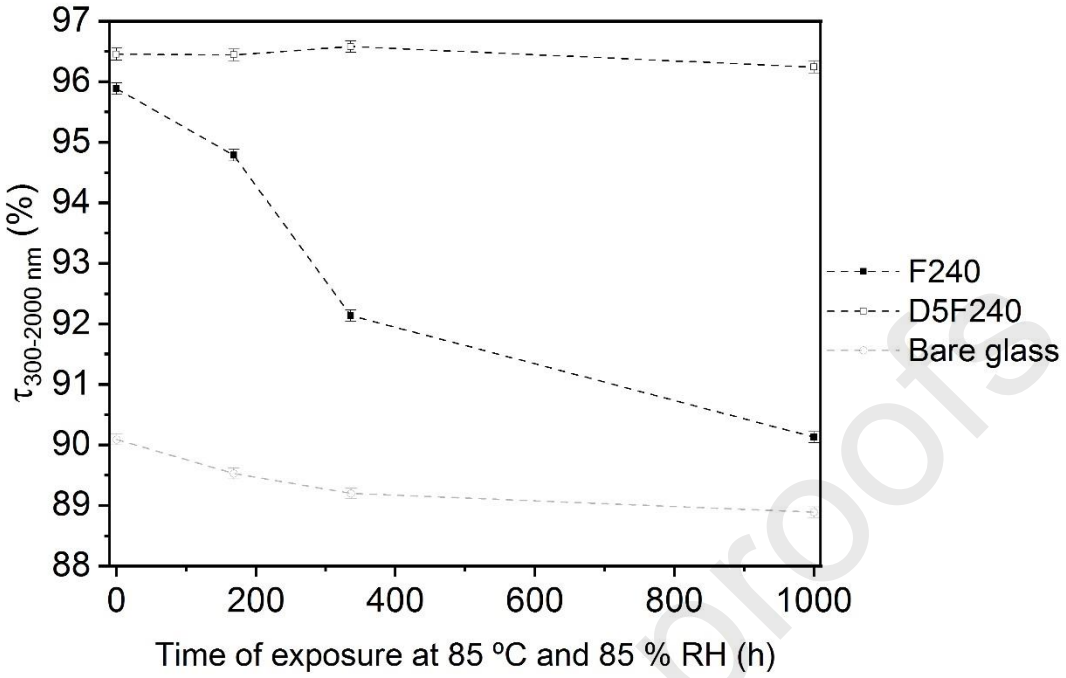

Figure 8. Evolution of integrated transmittance (300-2000 nm) of AR mono- and bi-layer stacks at different times of exposure to damp heat test conditions.

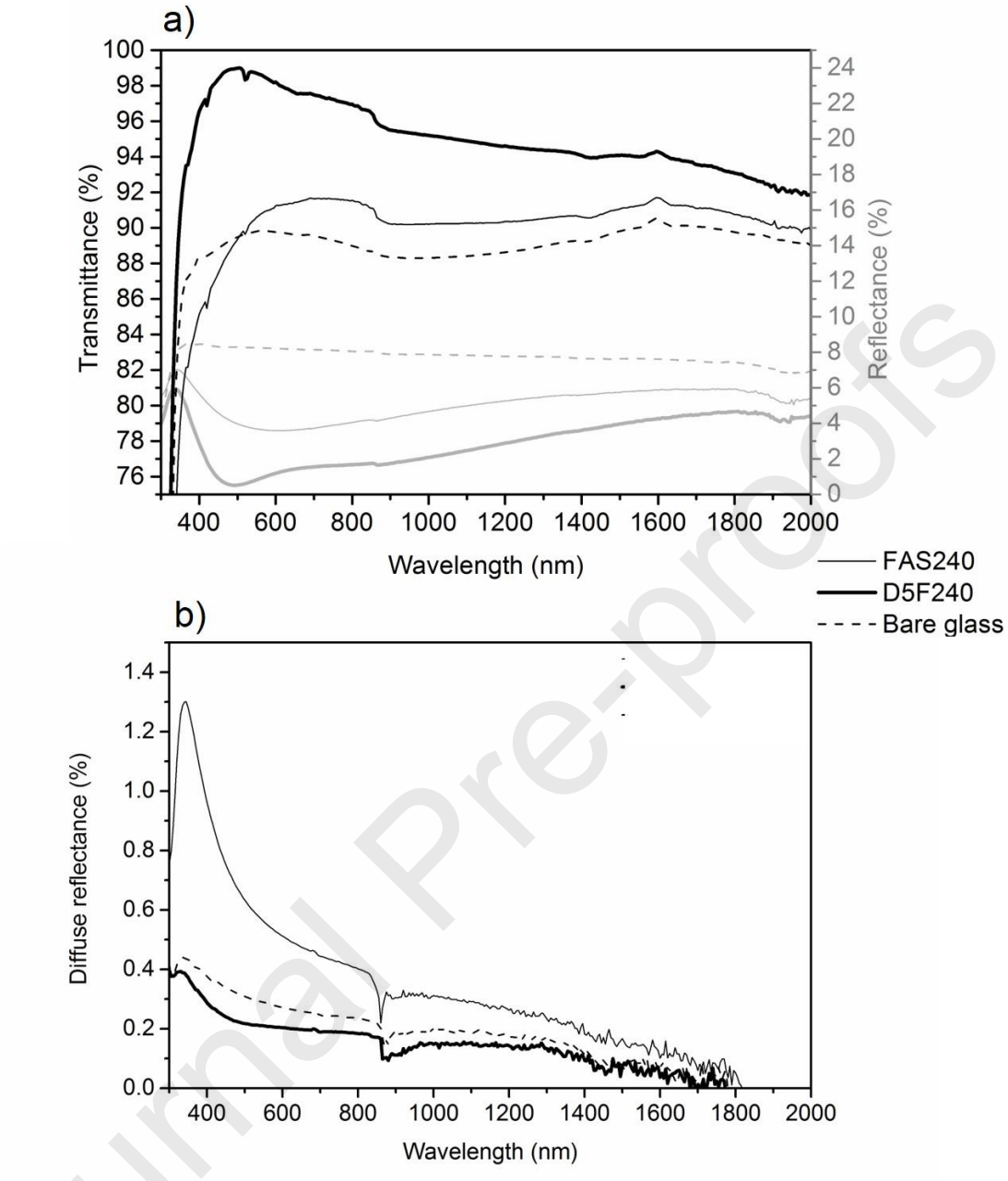

Figure 9. Total transmittance and reflectance (a) and diffuse reflectance (b) spectra of AR mono- and bi-layer stacks after 1000 h of exposure to damp heat test.

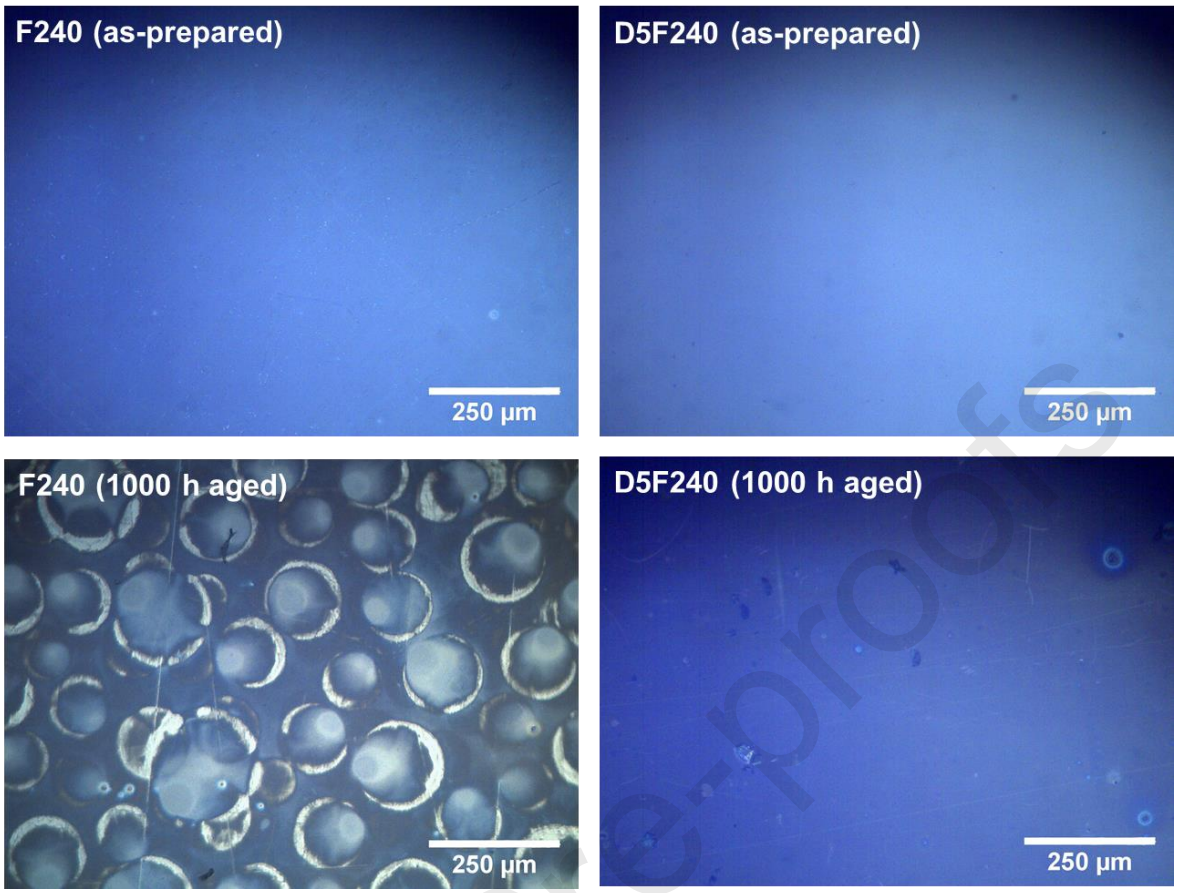

Figure 10. Optical microscope images (100X magnification) of AR mono- and bi-layer stacks surfaces before (as-prepared) and after 1000 h of exposure to damp heat test.

Table 7.

Thickness (d), refractive index (n) at 700 nm, auto loss of τ, τ gain over aged bare glass, and diffuse reflectance (ρ_{dif}) in the 300-2000 nm spectral range; and water contact angle ($\boldsymbol{\theta_c^{H_2O}}$) of AR layer stacks after damp heat aging.

Coating	d (nm)	n (700 nm)	Auto loss τ (%)	τ gain (%)	ρ_{dif} (%)	$\boldsymbol{\theta_c^{H_2O}}$ (º)
F240	95.4	1.31	6.0	1.4	0.5	113.0±0.8
D5F240	131.1*	1.22*	0.2	8.3	0.2	112.8±0.8

* External coating in D5F240

4. CONCLUSIONS

With the aim of overcoming the impact of soiling on an AR coating during its lifetime, a low surface energy coating was sought through the addition of fluoroalkyl silanes to a baseline silica sol-gel coating. This incorporation allowed the formation of a covalently bonded polyfluoroalkyl-silica network. The increase of a polyfluoroalkyl chain length linked to a silicon central atom produced an increase on hydrophobicity, accompanied by an increase of coating thickness and the decrease of integrated transmittance. This screening enabled the selection of the alkoxy silane with the longest non-hydrolyzable polyfluoroalkyl group for further optimization and the setting of the maximum applied temperature at 240 ºC.

Optimized polyfluoroalkyl-silica porous coatings were deposited as single AR mono-layers and as AR bi-layers stacked on both sides of low iron float glass, providing outstanding transmittance properties, achieving a gain of 7.1% in the case of the AR bi-layer stack. More specifically, the structure of the polyfluoroalkyl-silica porous coating was formed by grains that differed in size depending if the coating was deposited directly on glass or as an external coating on the dense silica coating. However, the surface free energy was similar, 19-20 mJ/m^2, for the desired low roughness values (R_q 0.6 nm) required for obtaining a low scattering of the incoming solar radiation.

Moreover, a highly remarkable outcome was related to the presence of the inner dense-structured coating sintered at high temperature in the AR bi-layer stack configuration prior to polyfluoroalkyl-silica porous coating growth. Apart from the given broadband antireflection behavior, this was the key to implement the required cohesive and adhesive resistance to withstand the stress provoked by the aggressive damp heat aging. The AR bi-layer stack offered inalterable optical constants and antireflection after 1000 h of exposure to damp heat conditions, as well as ultraviolet exposure, thermal cycling and humidity-freezing.

Acknowledgements

This work was supported by the Basque Government through EMAITEK 2017 program as well as the ELKARTEK projects FRONTIERS-2 (contract number KK2016-00093) and FRONTIERS-3 (contract number KK2017-00096).

The authors thank ICV-CSIC, Yolanda Castro and Alicia Durán for their support with ellipsometry and EEP measurements.

The authors thank Italian National Agency for New Technologies, Energy and Sustainable Economic Development (ENEA) for their collaboration with the aging tests.

The authors thank Miguel Pérez-Aradros for the help with graphical abstract illustration.

References

[1] K. Burrows, V. Fthenakis, Glass needs for a growing photovoltaics industry, Sol. Energy Mater. Sol. Cells. 132 (2015) 455–459. doi:10.1016/j.solmat.2014.09.028.

[2] A. Gombert, W. Glaubitt, K. Rose, J. Dreibholz, B. Blasi, A. Heinzel, D. Sporn, W. Doll, V. Wittwer, Antireflective transparent covers for solar devices, Sol. Energy. 68 (2000) 357–360. www.elsevier.com (accessed December 5, 2017).

[3] J. Moghal, J. Kobler, J. Sauer, J. Best, M. Gardener, A.A.R. Watt, G. Wakefield, High-Performance, Single-Layer Antireflective Optical Coatings Comprising Mesoporous Silica Nanoparticles, ACS Appl. Mater. Interfaces. 4 (2012) 854–859. doi:10.1021/am201494m.

[4] C. Agustín-Sáenz, J.Á. Sánchez-García, M. Machado, M. Brizuela, O. Zubillaga, A. Tercjak, Broadband antireflective coating stack based on mesoporous silica by acid-catalyzed sol-gel method for concentrated photovoltaic application, Sol. Energy Mater. Sol. Cells. 186 (2018) 154–164. doi:10.1016/j.solmat.2018.06.040.

[5] M. Vivar, R. Herrero, I. Antón, F. Martínez-Moreno, R. Moretón, G. Sala, A.W. Blakers, J. Smeltink, Effect of soiling in CPV systems, Sol. Energy. 84 (2010) 1327–1335. doi:10.1016/j.solener.2010.03.031.

[6] E. Muñoz, P.G. Vidal, G. Nofuentes, L. Hontoria, P. Pérez-Higueras, J. Terrados, G. Almonacid, J. Aguilera, CPV standardization: An overview, Renew. Sustain. Energy Rev. 14 (2010) 518–523. doi:10.1016/j.rser.2009.07.030.

[7] M. Castro, I. Antón, G. Sala, Pilot production of concentrator silicon solar cells: Approaching industrialization, Sol. Energy Mater. Sol. Cells. 92 (2008) 1697–1705. doi:10.1016/j.solmat.2008.08.001.

[8] M. Piliougine, C. Cañete, R. Moreno, J. Carretero, J. Hirose, S. Ogawa, M. Sidrach-De-Cardona, Comparative analysis of energy produced by photovoltaic modules with anti-soiling coated surface in arid climates, Appl. Energy. 112 (2013) 626–634. doi:10.1016/j.apenergy.2013.01.048.

[9] M. Sakhuja, J. Son, H. Yang, C.S. Bhatia, A.J. Danner, Outdoor performance and durability testing of antireflecting and self-cleaning glass for photovoltaic applications, Sol. Energy. 110 (2014) 231–238. doi:10.1016/j.solener.2014.07.003.

[10] W. Tang, Y. Huang, W. Meng, F. Qing, Synthesis of fluorinated hyperbranched polymers capable as highly hydrophobic and oleophobic coating materials, Eur. Polym. J. 46 (2010) 506–518. doi:10.1016/j.eurpolymj.2009.12.005.

[11] R. Kaseman, S. Brück, H. Schmith, Fluorine modification of ORMOCER (ORganically MOdified CERamics)-coating materials, Eurogel 91. (1992) 353–360.

[12] E.G. Shafrin, W.A. Zisman, Constitutive relations in the wetting of low energy surfaces and the theory of the retraction method of preparing monolayers, J Phys Chem. 1046 (1957) 519–524. doi:10.1021/j100834a002.

[13] T. Asefa, M.J. MacLachlan, N. Coombs, G.A. Ozin, Periodic mesoporous

organosilicas with organic groups inside the channel walls, Nature. 402 (1999) 867–871. doi:10.1038/47229.

[14] J.C. Brinker, Y. Lu, A. Sellinger, H. Fan, Evaporation-induced self-assembly: nanostructures made easy, Adv. Mater. 11 (1999) 579–585. doi:10.1002/(SICI)1521-4095(199905)11.

[15] M. Hikita, K. Tanaka, T. Nakamura, T. Kajiyama, A. Takahara, Super-liquid-repellent surfaces prepared by colloidal silica nanoparticles covered with fluoroalkyl groups super-liquid-repellent surfaces prepared by colloidal silica nanoparticles Covered with Fluoroalkyl Groups, Langmuir. 21 (2005) 7299–7302. doi:10.1021/la050901r.

[16] A. Nakajima, K. Abe, K. Hashimoto, T. Watanabe, Preparation of hard super-hydrophobic films with visible light transmission, Thin Solid Films. 376 (2000) 140–143. doi:10.1016/S0040-6090(00)01417-6.

[17] B.J. Basu, T. Bharathidasan, C. Anandan, Superhydrophobic oleophobic PDMS-silica nanocomposite coating, Surf. Innov. 1 (2013) 40–51. doi:10.1680/si.12.00013.

[18] R.N. Wenzel, Resistance of solid surfaces to wetting by water, Ind. Eng. Chem. 28 (1936) 988–994. doi:10.1021/ie50320a024.

[19] N.K. Adam, The physics and chemistry of surfaces, 3rd edit, Geoffrey Cumberlege, London, 1941.

[20] A.B.D. Cassie, S. Baxter, Wettability of porous surfaces, Trans. Faraday Soc. 40 (1944) 546–551.

[21] J.D. Miller, S. Veeramasuneni, J. Drelich, M.R. Yalamanchili, Effect of roughness as determined by atomic force microscopy on the wetting properties of PTFE thin films, Polym. Eng. Sci. 36 (1996) 1849–1855.

[22] B. van Ginneken, M. Stavridi, J.J. Koenderink, Diffuse and specular reflectance from

rough surfaces., Appl. Opt. 37 (1998) 130–9. doi:10.1364/AO.37.000130.

[23] C. Agustín Sáenz, O. Zubillaga Alcorta, M. Brizuela Parra, A broadband anti-reflective sol-gel coating composition, Patent application EP17382016, 2017.

[24] C. Agustín-Sáenz, M. Machado, A. Tercjak, Antireflective mesoporous silica coatings by optimization of water content in acid-catalyzed sol-gel method for application in glass covers of concentrated photovoltaic modules, J. Colloid Interface Sci. 534 (2019) 370–380. doi:10.1016/J.JCIS.2018.09.043.

[25] IEC 62108 International Standard, Concentrator photovoltaic (CPV) modules and assemblies - Design qualification and type approval, 2016.

[26] R.C. Buck, J. Franklin, U. Berger, J.M. Conder, I.T. Cousins, P. De Voogt, A.A. Jensen, K. Kannan, S.A. Mabury, S.P.J. van Leeuwen, Perfluoroalkyl and polyfluoroalkyl substances in the environment: terminology, classification and origins, Integr. Environ. Assess. Manag. 7 (2011) 513–541. doi:10.1002/ieam.258.

[27] R.J.H. Voorhoeve, Organohalosilanes, New York, 1967.

[28] D.K. Owens, R.C. Wendt, Estimation of the surface free energy of polymers, J. Appl. Polym. Sci. 13 (1969) 1741–1747.

[29] D.L. Wood III, C. Rulison, R.L. Borup, Surface properties of PEMFC gas diffusion layers, J. Electrochem. Soc. 157 (2010) B195–B206. doi:10.1149/1.3261850.

[30] ASTM G173-03, Standard tables for reference solar spectral irradiances: direct normal and hemispherical on 37º tilted surface, 2013. doi:10.1520/G0173-03R12.2.

[31] J.N. Helbert, Handbook of VLSI microlithography: principles, technology, and applications, Noyes Publications, 2001.

[32] A.L. Cauchy, Sur la réfraction et la réflexion de la lumière, Bull. Des Sci. Mathématiques. XIV (1830) 6–10.

[33] D.A.G. Bruggeman, Berechnung verschiedener physikalischer konstanten von

heterogenen substanzen. I. Dielektrizitätskonstanten und leitfähigkeiten der mischkörper aus isotropen substanzen, Ann. Phys. 24 (1935) 636–664. doi:10.1002/andp.19374210205.

[34] C. Boissière, D. Grosso, S. Lepoutre, L. Nicole, A.B. Bruneau, C. Sanchez, Porosity and mechanical properties of mesoporous thin films assessed by environmental ellipsometric porosimetry, Langmuir. 21 (2005) 12362–12371.

[35] M.R. Baklanov, K.P. Mogilnikov, V.G. Polovinkin, F.N. Dultsev, Determination of pore size distribution in thin films by ellipsometric porosimetry, J. Vac. Sci. Technol. B. 18 (2000) 1385. doi:10.1116/1.591390.

[36] D.L. Schmidt, B.M. DeKoven, C.E. Coburn, G.E. Potter, G.F. Meyers, D.A. Fischer, Characterization of a New Family of Nonwettable, Nonstick Surfaces, Langmuir. 12 (1996) 518–529. doi:10.1021/la9502913.

[37] A. Springsteen, Standards for the measurement of diffuse reflectance - An overview of available materials and measurement laboratories, Anal. Chim. Acta. 380 (1999) 379–390. doi:10.1016/S0003-2670(98)00576-5.

[38] D. Grosso, F. Cagnol, G.J.D.A.A. Soler-Illia, E.L. Crepaldi, H. Amenitsch, A. Brunet-Bruneau, A. Bourgeois, C. Sanchez, Fundamentals of mesostructuring through evaporation-induced self-assembly, Adv. Funct. Mater. 14 (2004) 309–322. doi:10.1002/adfm.200305036.

[39] M. Żenkiewicz, Methods for the calculation of surface free energy of solids, J. Achiev. Mater. Manuf. Eng. 24 (2007) 137–145.

[40] F.M. Fowkes, Attractive forces at interfaces, Ind. Eng. Chem. 56 (1964) 40–52.

[41] A. Grosjean, A. Soum-Glaude, P. Neveu, L. Thomas, Comprehensive simulation and optimization of porous SiO_2 antireflective coating to improve glass solar transmittance for solar energy applications, Sol. Energy Mater. Sol. Cells. 182 (2018)

166–177. doi:10.1016/j.solmat.2018.03.040.

[42] I. Petrina, A.B. Cueli, J. Moracho, A.R. Lagunas, CENER experience testing CPV modules, Energ. Int. 123 (2013) 68–71.

[43] C. Agustín-Sáenz, M. Machado, O. Zubillaga, A. Tercjak, Hydrophobic and spectrally broadband antireflective methyl-silylated silica coatings with high performance stability for concentrated solar applications, Sol. Energy Mater. Sol. Cells. 200 (2019) 109962. doi:10.1016/j.solmat.2019.109962.

Cecilia Agustín-Sáenz: Conceptualization, Investigation, Visualization, Writing- Original draft preparation.
Maider Machado: Supervision, Writing- Reviewing and Editing
Agnieszka Tercjak: Supervision, Writing- Reviewing and Editing

Declaration of interests

☒ The authors declare that they have no known competing financial interests or personal relationships that could have appeared to influence the work reported in this paper.

☐The authors declare the following financial interests/personal relationships which may be considered as potential competing interests:

HIGHLIGHTS:

- Polyfluoroalkyl-SiO_2 porous coating with proper tandem n-thickness was designed and characterized
- AR coatings with desired low surface energy, low roughness and low light scattering were deposited
- Hydrophobic film was only obtained for AR coatings with the longest polyfluoroalkyl chain
- Durability of the optical properties and hydrophobicity was achieved for the polyfluoroalkyl-SiO_2 AR bi-layer stack